15 Jun 2023

Hydrogen Gas Sensor Based On Seven-core Fiber Interference And Pt-WO3 Film

You Wang

Farhan Mumtaz
Missouri University of Science and Technology, mfmawan@mst.edu

Yutang Dai

Recommended Citation

Y. Wang et al., "Hydrogen Gas Sensor Based On Seven-core Fiber Interference And Pt-WO3 Film," *Materials Letters*, vol. 341, article no. 134245, Elsevier, Jun 2023.
The definitive version is available at https://doi.org/10.1016/j.matlet.2023.134245

Materials Letters 341 (2023) 134245

Contents lists available at ScienceDirect

Materials Letters

journal homepage: www.elsevier.com/locate/matlet

Hydrogen gas sensor based on seven-core fiber interference and Pt-WO_3 film

You Wang [a], Farhan Mumtaz [b,*], Yutang Dai [a,*]

[a] National Engineering Research Center of Fiber Optic Sensing Technology and Networks, Wuhan University of Technology, Wuhan 430000, China
[b] Department of Electrical and Computer Engineering, Missouri University of Science and Technology, Rolla, MO 65409-0040 USA

ARTICLE INFO

Keywords:
Fiber optic sensor
Pt-WO_3 thin film
Ellipsoidal balls
Spiral micro-grooves

ABSTRACT

Tungsten oxide (WO_3) typically owns the characteristics of electrochemical, photo-chromic, and gas-chromic. The seven-core fiber (SCF) generates a strong interference signal that comprises super-modes. The thermo-optic and thermo-expansion characteristics of SCF were utilized with an aid of Pt-WO_3 film that makes the sensor highly sensitive to the H_2 gas environment. The sensor with spiral micro grooves by femtosecond-laser ablation considerably enhanced the H_2 sensitivity from 3.28 nm/% to 4.0 nm/%, and obtained a response and recovery time < 90 s.

1. Introduction

Nowadays, preserving energy resources is a hot topic that is under discussion on the platform of researchers and scientists. H_2 gas is one of the major energy resources [1] and its overuse is extremely harmful due to its unrestrained and needless leakage into the environment. To overcome the leakage of energy resources, researchers have proposed a series of fiber-optic sensors and consequently, the demand for fiber-optic H_2 gas sensors in the energy sector is increasing day by day. Fiber-optic sensors are considered more suitable for H_2 gas detection and leakage loss prevention due to their unique advantages of robustness, reliability, and low cost. Fiber-optic H_2 sensors possess numerous features, such as intrinsically safe, anti-electromagnetic interference, chemical resistance, and small size [2]. Numerous fiber-optic sensors have been reported [3–7] with the deposition of hydrogen-sensitive films.

This letter reports first time best of our knowledge, a highly sensitive H_2 gas sensor based on SCF interference with sensitive Pt-WO_3 film. The sensor extends the feasibility of multi-core fiber-based structures for H_2 gas detection.

2. Experiment and results

2.1. Sensor preparation

In this work, two different sensors (S-1 and S-2) are reported for H_2 gas detection, as shown in Fig. 1(a, b), respectively. SCF (FIBRECORE, SM-7C1500) is used with core and cladding diameters of 6.1 μm and 125 μm, and their refractive indices are 1.4682 and 1.4628, respectively. SCF pitch distance between the center to the side core is 35 μm. A single-mode fiber (SMF-28e) is used as a lead-in fiber. The sensing length "*L*" is taken as 20 mm, and fabrication technique is reported in ref. [8]. A 50 nm thin film was sputtered at the end facet of the sensor using an ultra-high vacuum magnetron sputtering system (BESTECH). The following process was initiated for S-2, as S-1 was without micro-grooves structure.

Fs-laser system (IFRIT, Cyber Laser, Tokyo, Japan) with an operating wavelength of ~ 780 nm was employed to fabricate the spiral micro-grooves on the lateral surface of the SCF. The spiral micro-grooves were fabricated by using the following parameters: DC motor speed = 12 r/min, pulse energy = 20 uJ, repetition rate = 1000 Hz, scanning speed = 0.72 mm/min. After execution of the command, the spiral micro-grooves with a pitch distance of 60 μm and a depth of 16.7 μm were formed as shown in Fig. 1(e), and then etched by using 2% hydrofluoric acid for 1 min [3].

The Pt-WO_3 film was prepared by the hydrothermal method. A solution of Na_2WO_4 (0.66 g) and $H_2C_2O_4$ (0.18 g) was dissolved into distilled water (40 ml). HCl (3 mol/l) was added by drops until precipitation appeared. The prepared mixture was transferred into a Teflon-lined stainless autoclave and kept at 180 °C for 12 h. The resultant product was washed several times and dried at 70 °C. Subsequently, the platinum acetylacetone ($Pt(acac)_2$) and $WO_3{\cdot}2H_2O$ powder were mixed in a molar ratio of Pt:W::1:5 and then finely grounded. The mixture was

* Corresponding authors.
E-mail addresses: mfmawan@mst.edu (F. Mumtaz), daiyt6688@whut.edu.cn (Y. Dai).

https://doi.org/10.1016/j.matlet.2023.134245
Received 25 November 2022; Received in revised form 23 February 2023; Accepted 16 March 2023
Available online 21 March 2023

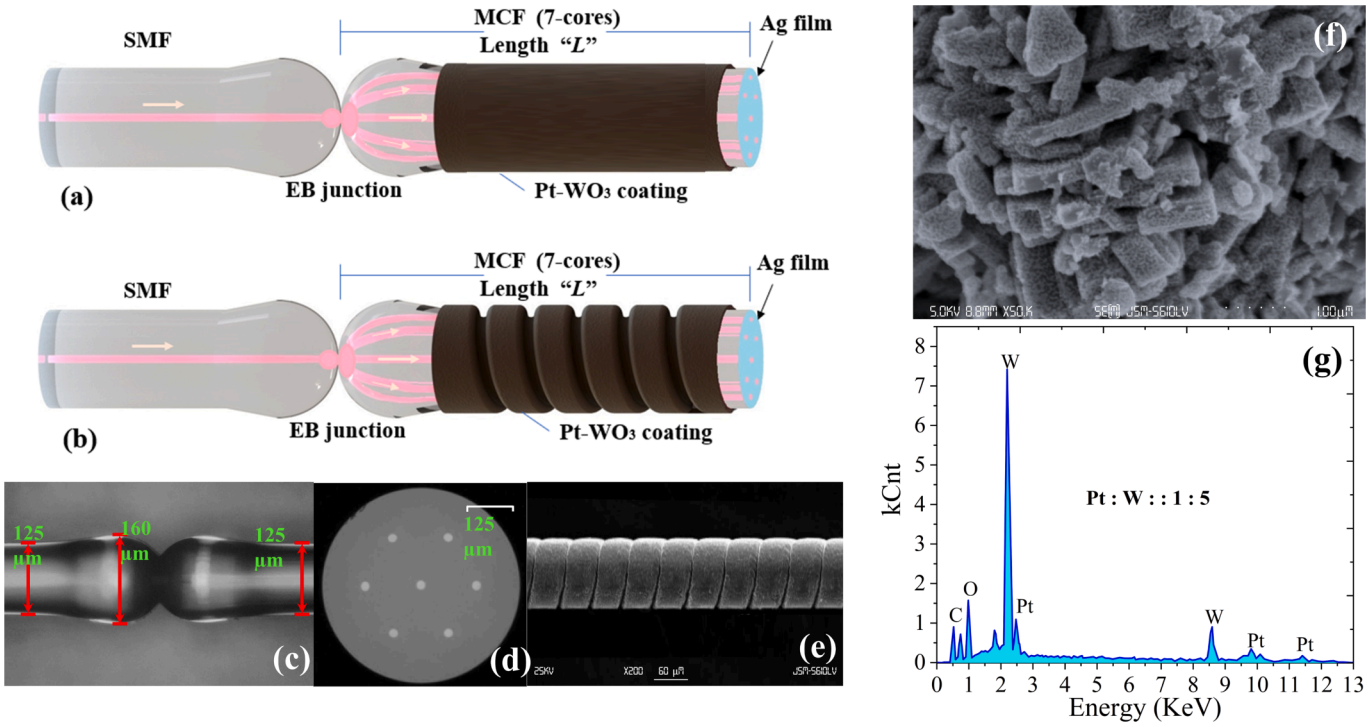

Fig. 1. Schematic of (a) S-1, (b) S-2; images under the microscopic show (c) EB junction, (d) SCF cross-section, (e) Fs-laser ablated spiral micro-groves, (f) Characterization of Pt-WO_3 film and (g) EDXS shows the profile of Pt-WO_3 film.

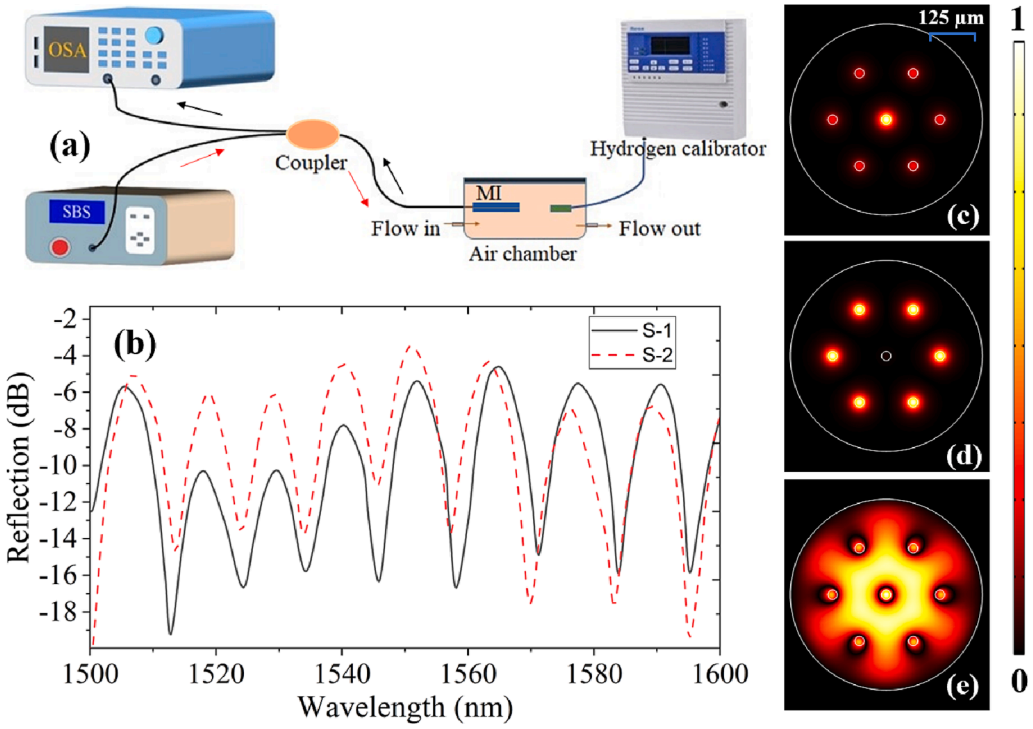

Fig. 2. (a) Schematic experimental setup, (b) reflection spectra for sensors S-1 and S-2, and simulated propagating modes profiles showing (c) center-core mode, (d) side-cores super-modes, and (e) cladding-modes.

annealed at 315 °C for 2 h. Finally, the product (Pt-WO_3) was mixed with deionized water, and applied evenly on the outer surface of SCF for S-1 and S-2, as shown in Fig. 1(a-b), respectively. The coated nanosheets of Pt-WO_3 were characterized by SEM, as shown in Fig. 1(f). It is observed that the WO_3 cluster was flaky with a thickness of about 10 to 20 nm, whereas the edge length was in the range of tens to hundreds of nm. Besides, platinum nanoparticles were uniformly distributed on the lamella surface, and numerous Pt-WO_3 nanosheets were stacked into a three-dimensional structure with a large number of gaps. Fig. 1(g) represents the recorded pattern by energy dispersive X-ray spectrometer

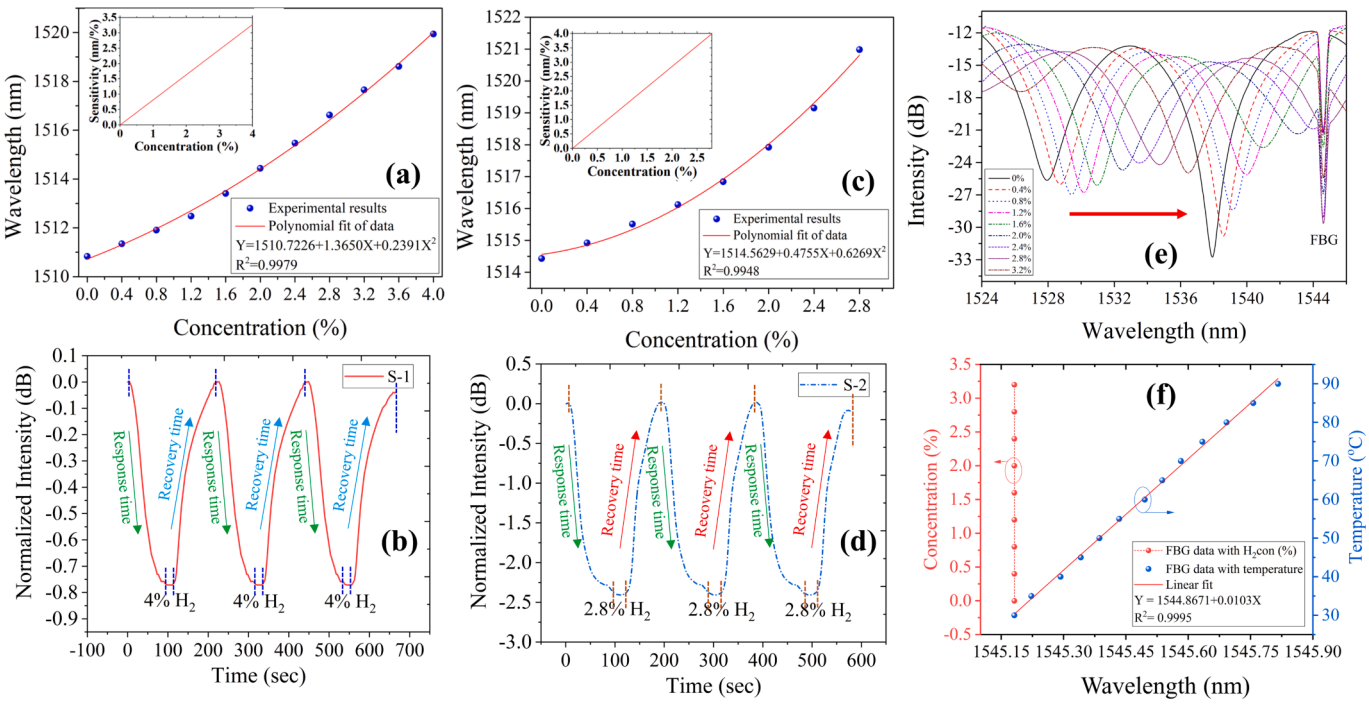

Fig. 3. Sensitivity fitting curve for (a) S-1 (c) S-2; Stability performance for (b) S-1 and (d) S-2; (e) FBG spectral evolution under different H_2 concentrations and (f) linear correlation of Bragg wavelength under different H_2 concentrations and different temperatures.

(EDXS) for Pt-WO_3 film where the atomic ratio was found: Pt:W::1:5, that is considered for higher sensitivity than other proportions of Pt-WO_3. The thickness of the Pt-loaded WO_3 film was approximately 2.0 μm, and the film is evenly distributed on the surface of sensors with strong adhesion.

2.2. Testing system and interference spectra

Fig. 2(a) portrays the schematic experimental setup employed for H_2 gas detection, while Fig. 2(b) exhibits the reflection spectra of S-1 and S-2 obtained through an optical spectrum analyzer (OSA, YOKOGAWA, AQ6370). A broadband light source with a flat wavelength range of 1520 nm to 1610 nm was employed to launch the light into the sensor via a 3 dB single-mode coupler. The proposed sensors generate a sequence of interferences in the reflection spectrum. For instance, ellipsoidal balls (EB) at the input triggered multimodal interference that affected cladding-modes interaction, whereas center-core mode was combined with side-core modes to stimulate super-mode propagational interferences, as exemplified in Fig. 2(c–e). The cumulative reflected intensity from the sensor can be estimated as follows [8],

$$I_{total} = I_c + \sum_{j=1}^{6} I_s^j + \sum_{i=1}^{M} I_{cl}^i + 2\sum_{j=1}^{6}\sqrt{I_c I_{cl}^i}\cos(\phi_i) + 2\sum_{j=1}^{6}\sum_{i=1}^{M}\sqrt{I_s^j I_{cl}^i}\cos(\phi_{i,j}) \quad (1)$$

where I_c, I_s, and I_{cl} represent center-core, side-core, and cladding-modes intensities. ϕ is the phase difference, and i and j denote the order of respective core and cladding modes.

2.3. S-1 performance

SCF is a Germanium-doped optical fiber and presents a high thermos-optic coefficient (6.83×10^{-7}/℃) and thermos-expansion coefficient (5.5×10^{-7}/℃) [8]. When the H_2 concentration increases in the air-sealed gas chamber, the deposited Pt-WO_3 film at the outer surface of the sensor reacts with the H_2 gas to generate a significant amount of heat, which changes the effective refractive index difference and sensing length of the sensor. The reflection spectrum for S-1 produces a red-shift with the increase of hydrogen concentration, and the sensitivity curve is plotted by monitoring the interference dip drift at $\lambda_N = 1511$ nm, as shown in Fig. 3(a). The inset indicates that the sensitivity of the sensor is non-linear corresponding to H_2 concentration vs sensitivity, and obtained sensitivity for S-1 is 3.28 nm/% in the H_2 concentration range of 0–4%, with an excellent fitting of $R^2 = 0.9979$.

The stability of S-1 is measured by an optical power meter instead of OSA which shows response and recovery time in real-time, as shown in Fig. 3(b). It was observed that the sensor produces highly stable performance and exhibits a response and recovery time of < 100 sec.

2.4. S-2 performance

Likewise, S-2 produces red-shift in reflection spectra with the increase of H_2 concentration. The sensitivity curve for S-2 is fitted by tracing the interference dip wavelength of $\lambda_N = 1514$ nm at different H_2 concentrations, as shown in Fig. 3(c). The spiral micro-structure in S-2 sensor increases the reaction area between hydrogen gas and SCF via Pt-WO_3 film, and resultantly enhances SCF ductility during heat reaction, thus promoting sensing performance. The sensitivity of the sensor increases linearly when the H_2 concentration gradually increases from 0% to 2.8%, and the maximum sensitivity for S-2 reaches 4 nm/% with excellent polynomial fitting, i.e., $R^2 = 0.9948$, as shown in the inset of Fig. 3(c). S-2 shows high sensitivity but less range of H_2 concentration compared to S-1. The sensitivity is enhanced due to the spiral micro-grooves structuring in S-2. S-2 also demonstrates a stable response and exhibits a response and recovery time < 90 sec, as shown in Fig. 3(d). S-2 equally possesses the feasibility of reusing after reacting with H_2 concentrations when its original state is restored.

2.5. Temperature compensation

To eliminate the temperature cross-sensitivity of the sensor, an FBG was cascaded with the sensor. The FBG was placed in close proximity to the H_2 calibrater for capturing the temperature profile during the H_2 test. Fig. 3(e) shows that FBG was unaffected by H_2 gas. Bragg

Table 1
Comparison of the proposed H_2 sensor.

Structure type		Detection range H_2/%	Sensitivity (nm/%)	Response time (sec)	Recovery time (sec)
FBG with spiral[3]		0.02–4	0.522	180	78
FBG [4]		0.02–1	0.536	60	120
SMF-HCF-LMAF [5]		0–2.4	1.04	78	78
MZI [6]		0–5	1.2	–	–
This work	**S-1**	**0–4**	**3.28**	**<100**	**< 100**
	S-2	**0–2.8**	**4**	**< 90**	**< 90**

wavelength of FBG was shifted linearly with temperature rise when it was tested into heating furnance, yielding a sensitivity of 0.01 nm/°C, as expected. The linear response of FBG with different H_2 concentrations and temperatures is plotted in Fig. 3(f). Therefore FBG cascade with sensor eliminate temperature cross-talk while H_2 detection.

Finally, a comparison is made with the earlier reported sensor, as given in Table. 1, which confirms the utilization of the proposed sensor has great potential to become part of the real H_2 gas environment for continuous monitoring.

3. Conclusion

In summary, the H_2 sensors based on SCF interference signal with Pt-WO_3 film and Fs-laser ablated micro-structuring are experimentally demonstrated. The experimental results indicate that the sensor displayed optimum sensitivity of 4 nm/% with a highly stable response. Also, the sensor compensates temperature cross-talk using FBG. The proposed sensor opens new possibilities of using SCF in the sensor for H_2 environment monitoring.

CRediT authorship contribution statement

You Wang: Methodology, Investigation, Writing – original draft. **Farhan Mumtaz:** Conceptualization, Methodology, Software, Validation, Investigation, Writing – review & editing. **Yutang Dai:** Conceptualization, Validation, Project administration, Supervision, Writing – review & editing.

Declaration of Competing Interest

The authors declare that they have no known competing financial interests or personal relationships that could have appeared to influence the work reported in this paper.

Data availability

No data was used for the research described in the article.

Acknowledgment

This work was financially supported by National Natural Science Foundation of China, NSFC (No. 51975442 and No. 61475121).

References

[1] L. Nie, X. Guo, C. Gao, X. Wu, J. Chen, L. Peng, Fabrication and optical hydrogen gas sensing property of hierarchical WO3 Porous/Nanowires film, Mater. Lett. 314 (2022), 131805, https://doi.org/10.1016/j.matlet.2022.131805.
[2] K. Chen, D. Yuan, Y. Zhao, Review of optical hydrogen sensors based on metal hydrides: recent developments and challenges, Opt. Laser Technol. 137 (2021), 106808, https://doi.org/10.1016/j.optlastec.2020.106808.
[3] X. Zhou, Y. Dai, M. Zou, J.M. Karanja, M. Yang, FBG hydrogen sensor based on spiral microstructure ablated by femtosecond laser, Sens. Actuators, B Chem. 236 (2016) 392–398, https://doi.org/10.1016/j.snb.2016.06.027.
[4] J. Dai, M. Yang, Z. Yang, Z. Li, Y. Wang, G. Wang, Y. Zhang, Z. Zhuang, Performance of fiber Bragg grating hydrogen sensor coated with Pt-loaded WO3 coating, Sens. Actuators, B Chem. 190 (2014) 657–663, https://doi.org/10.1016/j.snb.2013.08.083.
[5] Y. Li, C. Zhao, B. Xu, D. Wang, M. Yang, Optical cascaded Fabry-Perot interferometer hydrogen sensor based on vernier effect, Opt. Commun. 414 (2018) 166–171, https://doi.org/10.1016/j.optcom.2017.12.012.
[6] F. Zhou, S.J. Qiu, W. Luo, F. Xu, Y.Q. Lu, An all-fiber reflective hydrogen sensor based on a photonic crystal fiber in-line interferometer, IEEE Sens. J. 14 (2014) 1133–1136, https://doi.org/10.1109/JSEN.2013.2293347.
[7] M. Wang, M. Yang, J. Cheng, J. Dai, M. Yang, D.N. Wang, Femtosecond laser fabricated micro Mach-Zehnder interferometer with Pd film as sensing materials for hydrogen sensing, Opt. Lett. 37 (2012) 1940, https://doi.org/10.1364/ol.37.001940.
[8] F. Mumtaz, Y. Dai, H. Wenbin, L.G. Abbas, R. Parveen, M.A. Ashraf, A weakly coupled multi-core fibre-based Michelson interferometer composed of an in-fibre coupler, Opto-Electron. Rev. 29 (2021) 117–125, https://doi.org/10.24425/opelre.2021.139436.